Check for updates

Activation of peroxymonosulfate for rhodamine-B removal from water: enhanced efficiency with cobalt-enriched, magnetically recoverable CNTs

M. O. Abdel-Salam, [ID] †[abc] Hebatullah H. Farghal, [ID] †[a] Ehab El Sawy, [ID] [a] Taeho Yoon [ID] *[d] and Mayyada M. H. El-Sayed [ID] *[a]

Dyes are known to pose environmental threats due to their mutagenic and persistent effects. To address this concern, researchers have explored various unconventional dye degradation materials, such as metal oxides with carbon materials. However, challenges related to degradation efficiency and regeneration have been significant obstacles. Consequently, there has been a surge in interest in recent years toward using nanomaterials with carbon materials activated by peroxymonosulfate for organic pollutant degradation. In this study, we present a novel approach to prepare a hybrid nanocomposite catalyst, $CoS/CoFe_2O_4$-CNTs (CS/CF-CNTs), using a carbon nanotube decorated with cobalt ferrite and further enhanced by embedding with cobalt sulfide nanoflowers. This catalyst aims at enhancing Rhodamine-B degradation through advanced oxidation processes. The carbon nanotubes provide a stable substrate for the cobalt materials, with cobalt ferrite (CF) serving as a magnetic component, facilitating catalyst removal and regeneration for multiple uses. Due to the oxidation involved in the degradation process, high electronic conductivity of the carbon nanotubes and the active cobalt sites of the composite play a crucial role in activating peroxymonosulfate to generate reactive oxygen radicals. Notably, the CS/CF-CNTs catalyst showed a remarkable Rhodamine-B degradation rate of 98% in less than 10 min. The catalyst also exhibited excellent stability even after four cycles of regeneration. The operating reaction conditions were optimized by investigating the effects of pH, dye concentration, salinity with different salts, catalyst dose, and peroxymonosulfate dose, and the results demonstrated the superior effectiveness of CS/CF-CNTs compared to CS and to CF-CNTs, emphasizing the synergistic interaction between the carbon nanotubes and the two cobalt materials. Quenching experiments revealed the involvement of sulfate and hydroxyl radicals in the degradation reaction mechanism.

[a]*Department of Chemistry, School of Sciences and Engineering, The American University in Cairo, Cairo, 11835, Egypt. E-mail: mayyada@aucegypt.edu*

[b]*Analysis and Evaluation Department, Egyptian Petroleum Research Institute (EPRI), 1 Ahmed El Zomor St., Nasr City, Cairo, 11727, Egypt*

[c]*Central Analytical Laboratories, Egyptian Petroleum Research Institute (EPRI), Nanotechnology Research, 1 Ahmed El Zomor St., Nasr City, Cairo, 11727, Egypt*

[d]*Department of Chemical Engineering, Kyung Hee University, Yongin-si, Gyeonggi-do, 17104, Republic of Korea. E-mail: tyoon@khu.ac.kr*

† Authors contribute equally to the work.

1. Introduction

Water is an instrumental natural resource for the existence of humans and living organisms. Despite its importance, all living organisms are facing the serious problems of water shortage and pollution. Water pollution arises from domestic, sewage, agricultural, and industrial wastewater.[1] Among the contaminants of great concern nowadays are the emerging contaminants. These are found in water at minute concentrations that can only be detected using sophisticated analytical instruments and could pose health hazards with prolonged exposure. Examples of emerging contaminants are pharmaceuticals and personal care products, pesticides, disinfectants, and others.[2] This study is concerned with the emerging contaminant Rhodamine-B, which is a basic dye that is used in the textile industry. It is carcinogenic and neurotoxic through inhalation and ingestion.[3] The value of the Rhodamine-B market in 2023 was 182.37 million USD, and it is expected to rise to 252.89 million USD in 2033 (Spherical insights, **https://www.sphericalinsights.com/reports/rhodamine-b-market**, accessed May 6th, 2024). It is persistent in the environment, with high stability and minimal degradation tendency.[4] The concentration of Rhodamine-B in textile wastewater in Hayatabad Peshawar, Khyber Pakhtunkhwa, Pakistan was found to be in the range of 20–250 mg L^{-1}.[5] Different methods have been utilized for the removal of Rhodamine-B from wastewater, such as adsorption,[6] membrane filtration[7] and advanced oxidation processes.[8] The method applied herein is an advanced oxidation process; these processes are characterized by the generation of strong hydroxyl or sulfate radicals that can degrade even

the most recalcitrant contaminants in various types of waste-water.[9] Various methods have been applied for the generation of radicals, including the conventional chemical method, along with other modern sonochemical, photochemical, and electro-chemical techniques. Chemical methods deploy ozone, hydrogen peroxide, and persulfate, which are not effective on their own, but require activation.[10] Herein, the chemical method is applied using the oxidant peroxymonosulfate or oxone (PMS). PMS can be activated via UV light or heat treatment. Alternatively, less-energy-intensive transition-metal-induced activation can be conducted using homogeneous or heterogeneous catalysts. Heterogeneous catalysts are preferable to homogeneous catalysts, as the former have less toxicity and are more recyclable.[11] Rhodamine-B was efficiently and almost completely degraded by Fe/MCM-41 catalysts in the presence of H_2O_2 at an initial dye concentration of 100 ppm, 1 g L^{-1} catalyst dose, H_2O_2 dose of 20 mmol L^{-1}, pH 4, and temperature of 80 °C.[12]

In this work, cobalt sulfide/cobalt ferrite-carbon nanotubes (CS/CF-CNTs) catalysts are combined with PMS to potentially enhance the degradation of Rhodamine-B. Cobalt-based heterogeneous catalysts are known for their superiority over the Fenton system and higher standard potential compared to other transition metals.[13] The presence of cobalt ferrite should impart magnetic properties to the composite, facilitating its collection from wastewater via a magnetic field after the degradation process. Carbon nanotubes are deployed due to their excellent surface area, catalytic properties, and electron transfer ability, which makes them good candidates for water treatment.[14] Numerous reports have shown the superior performance of cobalt-based heterogeneous catalysts combined with PMS. For example, a cobalt/MOF with PMS degraded about 98% of 20 ppm Rhodamine-B in 30 min.[15] Additionally, CoCN–NaBH$_4$ (Co(OH)$_2$–g-C$_3$N$_4$) was able to degrade almost 100% of 100 ppm orange G at a catalyst dose of 0.1 g L^{-1} and a PMS dose of 0.23 mM.[16]

This is the first report, to the best of our knowledge, on the degradation of Rhodamine-B using cobalt sulfide/cobalt ferrite-carbon nanotubes. This work investigates the surface morphologies and physicochemical properties of the CS/CF-CNTs hybrid nanocomposite catalyst using various techniques, such as X-ray diffraction, scanning electron microscopy, transmission electron microscopy, X-ray photoelectron spectroscopy, and nitrogen adsorption–desorption isotherms. A comprehensive study is conducted on the effect of the different operating parameters on the removal, including pH, contact time, initial concentration, catalyst dose, PMS dose, and salinity with different salts. The selectivity of the catalyst and PMS toward Rhodamine-B is tested in tap water and compared to that in distilled water. In addition, the reusability of the catalyst is assessed, and the removal mechanism is explained in view of the findings of the quenching experiments.

2. Materials and methods

2.1. Materials

Oxone (PMS; 2KHSO$_5$), ferric nitrate nonahydrate (Fe(NO$_3$)$_3$·9H$_2$O), ethanol (C$_2$H$_5$OH), cobalt(II) nitrate hexahydrate

(Co(NO$_3$)$_2$·6H$_2$O), acetic acid sodium salt (CH$_3$COONa), sulfuric acid (H$_2$SO$_4$), nitric acid (HNO$_3$), ethylene glycol (C$_2$H$_6$O$_2$), and methanol (CH$_3$OH) were purchased from Sigma-Aldrich (99% analytical grade). Thiourea (H$_2$NCSNH$_2$), sodium chloride (NaCl), and potassium sulfate (K$_2$SO$_4$) were purchased from Duksan Pure Chemicals Co., Ltd (95% analytical grade). CNTs were obtained from Korea Nano Company. Rhodamine-B was obtained from Loba Chemie, PVT, LTD. All the reagents were of analytical grade and were used as obtained. All the solutions were prepared using ultrapure water.

2.2. Preparation of the CS/CF-CNTs hybrid nanocomposite

A CS/CF-CNTs hybrid nanocomposite was synthesized using a solvothermal technique. Initially, 357 mg of Co (NO$_3$)$_2$·6H$_2$O were dissolved in 75 mL of C$_2$H$_6$O$_2$ and ultrasonicated for 10 min to achieve complete dispersion. Subsequently, 252 mg of H$_2$NCSNH$_2$ were added to the mixture while ultrasonication continued. A solution of magnetic-CoFe$_2$O$_4$-CNTs, prepared using the procedure outlined in our previous report,[11] was then added dropwise to the sonicated mixture. After 1 h of agitation, the resulting solution was transferred to a 100 mL polytetrafluoroethylene-lined autoclave. The reaction mixture underwent heating at 180 °C for 12 h in an oven, followed by cooling to room temperature as depicted in Fig. 1. The resultant black precipitate, identified as the CS/CF-CNTs composite, was washed three times with distilled water and subsequently dried in a vacuum oven at 70 °C for 6 h. CoS was synthesized using a similar procedure, excluding the addition of magnetic CoFe$_2$O$_4$-CNTs.

2.3. Characterization of the as-synthesized (CS/CF-CNTs) nanocomposites

Various analytical techniques were employed to examine the hybrid nanocomposite prepared in this study. The crystalline structures of the samples were analyzed using X-ray diffraction (XRD) with Cu Kα radiation at 40 kV and 30 mA, scanning angles within the range of 10–70°, and a scan step of 0.02° (PANalytical, X'Pert-PRO MPD). High-resolution transmission electron microscopy (HR-TEM) at 200 kV (FEI Tecnai G2F20) and field emission scanning electron microscopy (FE-SEM) (Hitachi-Japan, S-4800) were used to investigate surface morphologies. X-ray photoelectron spectroscopy (XPS) with Al Kα mono-chromatized radiation (AXIS Nova) was employed to analyze the surface configuration and components of the samples. Infrared (IR) spectra were collected using a total reflectance infrared (ATR-IR) spectrometer (Bruker Instruments) in the range of 4000–400 cm^{-1} at a resolution of 4 cm^{-1}. The degradation of Rhodamine-B was monitored using a Cary UV-vis Agilent G51911AA spectrophotometer. Furthermore, the hybrid nano-composite sample underwent examination using a nitrogen adsorption–desorption apparatus (Micromeritics 3FlexSurface Characterization Analyzer) at −196 °C. Additionally, the Bru-nauer–Emmett–Teller (BET) surface area and pore size distri-bution (PSD) were estimated. The sample was degassed at 180 °C for 12 h before conducting the adsorption–desorption experiments. The magnetic properties of the samples were
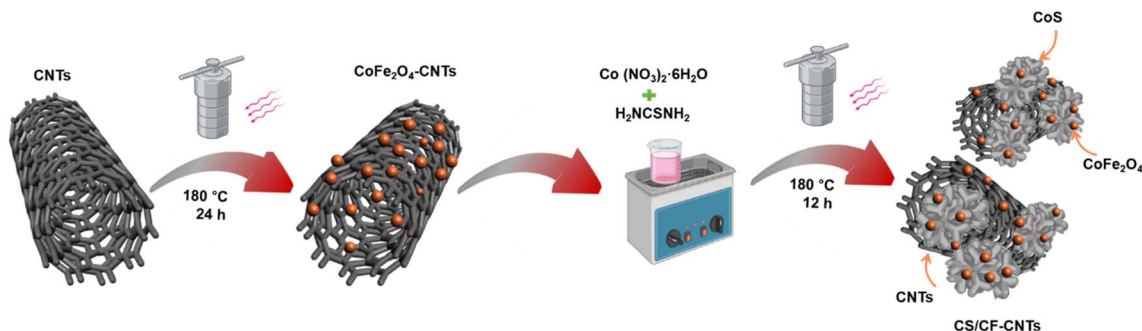
Fig. 1 Schematic diagram of the synthesis of CS/CF-CNTs.

measured using a Lake Shore VSM 7307 vibration magnetometer. The PSD was determined using the Barrett–Joyner–Halenda (BJH) methodology, and the BET-specific surface area was calculated using the BET equation. Zeta potential measurements were performed at pHs from 3.1 to 11.1 to determine the charge of the catalyst at various pH values.

2.4. Evaluating the catalytic degradation of CS/CF-CNTs with PMS activation

Catalytic degradation was studied at different catalyst and PMS doses in 100 mL of a 50 ppm Rhodamine-B solution without adjusting the pH (pH was about 3.3). The study was extended using various initial concentrations (10–50 ppm) of the dye in the presence of 10 mg catalyst and 60 mg PMS without pH adjustment. Similarly, the degradation kinetics were examined under the same conditions. The effect of pH was investigated in the range of 3.3–9.4 using the same catalyst and PMS doses indicated earlier. After degradation, 5 mL of the contaminant solution was quenched with 5 mL of sodium thiosulfate (0.5 M) and measured on a UV/VIS spectrophotometer at 554 nm. The obtained absorbance was substituted in a calibration curve to determine the remaining concentration, and the percent removal was determined as follows:

$$\%\text{Removal} = \frac{C_0 - C_r}{C_0} \times 100$$

where C_0 is the initial concentration of Rhodamine-B, while C_r is the concentration of Rhodamine-B remaining after catalytic degradation.

2.5. Testing the regenerability, selectivity, and stability of the nanocomposite

A regeneration study was conducted over four successive cycles. In each cycle, 100 mL of a 10 ppm solution of Rhodamine-B was used at 0.1 g L^{-1} catalyst dose and 0.6 g L^{-1} PMS dose. Upon the completion of each catalytic degradation cycle, the CS/CF-CNTs hybrid nanocomposite catalyst was separated by applying an external magnetic field and then thoroughly washed with 10 mL of deionized water and dried overnight at 70 °C before commencing the subsequent recyclability experiment. The degradation efficiency of the catalyst in the presence of PMS was tested on 10 ppm Rhodamine-B in tap water and compared to

that in distilled water. Additionally, the selectivity of the catalyst in the presence of PMS was tested on 50 ppm Rhodamine-B in the presence of salts such as NaCl and K$_2$SO$_4$ at 5 mM concentration.

Quenching experiments were used to explore the underlying mechanism of pollutant degradation by identifying the reactive species responsible for the process. In this study, *tert*-butyl alcohol (TBA, 1 M) and ethanol (1 M) were utilized as quenching agents to differentiate between the hydroxyl radicals (˙OH) and sulfate radicals (SO$_4$˙$^-$) that are potentially involved in the degradation of Rhodamine-B. TBA selectively scavenges hydroxyl radicals due to its higher reactivity with ˙OH (rate constant ≈ 3.8–7.6×10^8 M^{-1} s^{-1}) compared to its relatively slow interaction with sulfate radicals (rate constant ≈ 4–9.1×10^5 M^{-1} s^{-1}). Conversely, ethanol acts as a dual scavenger, reacting with hydroxyl and sulfate radicals, but with different rate constants. This difference in bahavior enables a clearer understanding of which reactive species dominate under the applied experimental conditions. The quenching experiments were performed using a catalyst dosage of 10 mg, 60 mg of PMS, and a pollutant concentration of 50 mg L^{-1} Rhodamine-B in a reaction volume of 100 mL. To examine the catalyst's stability during Rhodamine-B degradation, leaching tests for cobalt and iron ions were conducted. The concentrations of leached cobalt and iron ions were measured using Inductively Coupled Plasma Optical Emission Spectroscopy (ICAP™ 7400 Duo, Bremen, Germany, ICP). Before analysis, calibration curves were constructed to quantify the metal ions precisely, with the detection wavelengths set at 371.993 nm for iron and 350.228 nm for cobalt.

3. Results and discussion

3.1. Characterization of the nanocatalysts

XRD analysis was conducted to examine the crystalline structure of the hybrid nanocomposite and identify the specific phases (Fig. 2). In the XRD pattern of the CNTs, notable peaks were observed at 26° and 43°, corresponding to the (0 0 2) and (1 0 0) planes, respectively. These peaks indicate the presence of concentric cylindrical features in the CNTs and suggest adequate graphitization with sp^2-type atoms, devoid of carbon-based impurities or catalytic metal particles on their surfaces.[17] For the CF-CNTs, distinct diffraction peaks were observed at
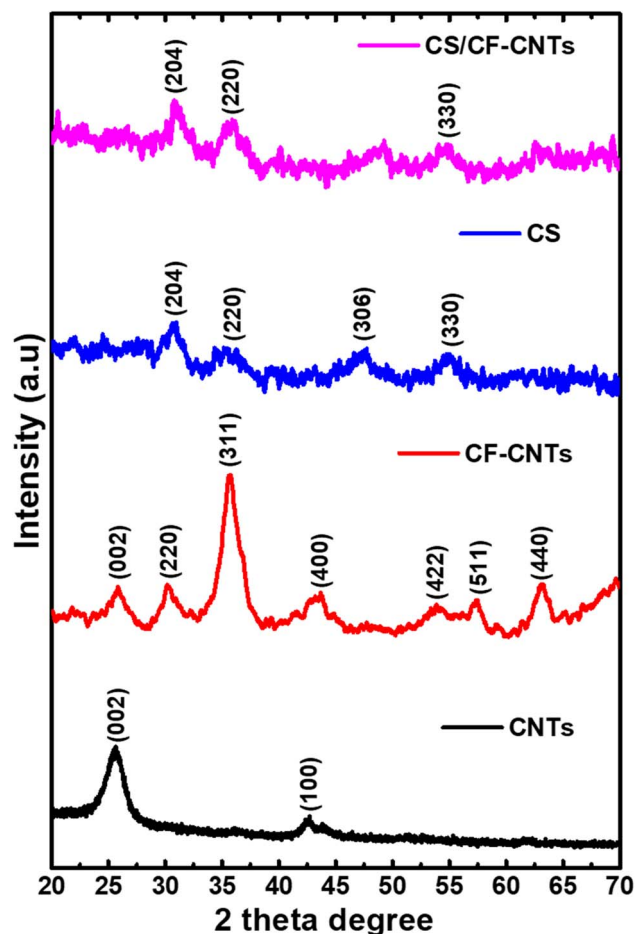
Fig. 2 XRD patterns of CNTs, CF-CNTs, CS, and CS/CF-CNTs nanocomposite.

31.3°, 36.1°, 43.3°, 53°, 57.4°, and 63.5°, corresponding to the (2 2 0), (3 1 1), (4 0 0), (4 2 2), (5 1 1), and (4 4 0) diffraction planes, respectively. These peaks are characteristic of the spherical spinel single-phase CF.[11,18] For the CS sample, the diffraction peaks appear at 31.05°, 35.68°, 47.13°, and 54.91° with low intensity, indicating the amorphous or nanocrystalline structure of CS, and these peaks correspond to the (204), (220), (306) and (330) planes, respectively.[19] In the XRD pattern of the CS/CF-CNTs, the intensity slightly increased with a small shift at

47.13°, and the graphitic carbon peak could not be seen as a well-defined peak. This could be attributed to the characteristic (0 0 2) peak of graphitic carbon being weak, indicating that the carbon structures in CNTs are disordered. This observation aligns with previous reported findings.[20]

To scrutinize its morphological structure, FE-SEM and HR-TEM analyses were conducted on the synthesized CS/CF-CNTs hybrid nanocomposite. As depicted in Fig. 3a, the morphology of the pristine CS exhibited a micro-flower-like structure,[21] with spherical CF firmly anchored on the cylindrical structure of the CNTs and CS. The hydrothermal method seems to have facilitated the effective loading of CF onto the surfaces of the CNTs and CS. Fig. 3b presents the HR-TEM image of the CS/CF-CNTs hybrid nanocomposites, revealing the intertwining of CS with the CNT networks. Similar observations were demonstrated in the FE-SEM images. The successful fabrication of the CS/CF-CNTs hybrid nanocomposite is evident from the absence of free CF in the HR-TEM images and FE-SEM micrograph.

XPS analysis was employed to determine the valence state and elemental composition of the CS/CF-CNTs hybrid nanocomposites. The survey spectrum in Fig. 4a indicates the presence of Co, Fe, S, O, and C in the energy region, which is consistent with the XRD results. Further analysis of the Co 2p spectrum (Fig. 4b) based on the Gaussian fitting approach reveals two peaks at 785 and 802.8 eV, which correspond to the satellite peaks of Co^{2+},[22] along with peaks at 778.5 and 793.7 eV corresponding to the Co $2p_{3/2}$ and $2p_{1/2}$ of cobalt sulfide.[23] The peaks at 780.6 and 796.3 eV suggest the coexistence of Co^{3+} and Co^{2+}, with Co^{3+} potentially providing additional active sites for degradation. The Fe $2p_{3/2}$ spectrum (Fig. 4c) shows peaks at 711.94, 716.8, 721.2, and 737 eV, indicating the Fe^{3+} and Fe^{2+} states. The S 2p spectrum (Fig. 4d) displays peaks at 168.5 eV (oxidized S), 164.5 and 162.5 eV (S–C bond), and 161.8 eV (CoS).[24,25] In addition, Fig. 4e presents the high-resolution C 1s spectrum of the nanocomposites. The high-resolution C 1s spectrum (Fig. 4e) reveals peaks at 284.4 eV (C–C/C≡C bonds), 288.5 eV (O–C–O), and 285.31 eV (C–O/C–S),[26] confirming tight bonding between C atoms and S atoms, indicating the attachment of CoS particles to the surface of the CNTs. Fig. 4f presents the deconvolution of the O 1s energy region. The two evident components have been attributed to the contribution of the crystal lattice oxygen (lower binding energy) and chemisorbed oxygen species (higher binding energy). The appearance of the
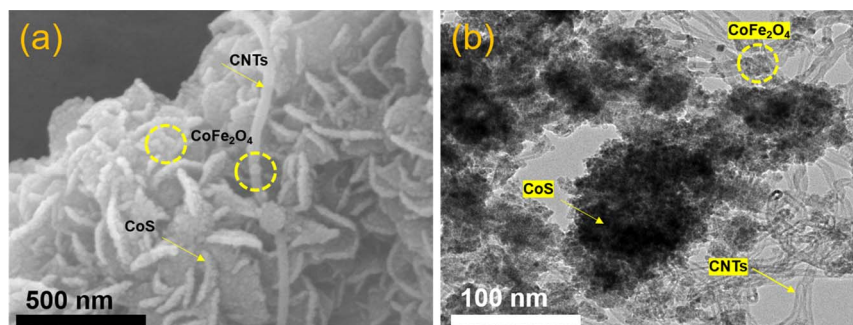

Fig. 3 (a) SEM images and (b) HR-TEM images of CS/CF-CNTs nanocomposite.
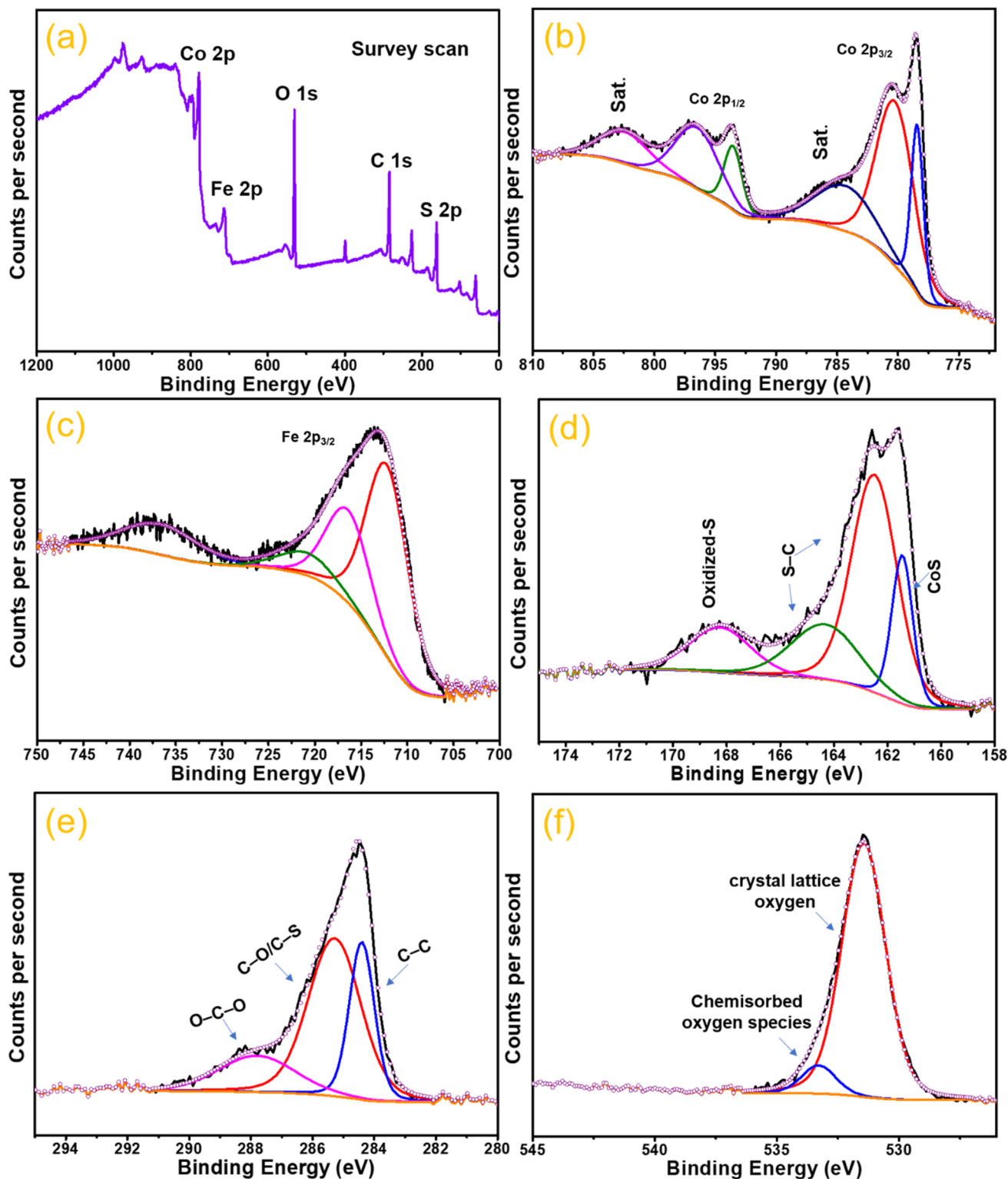
Fig. 4 XPS spectra of CS/CF-CNTs: (a) survey spectrum, (b) Co 2p, (c) Fe 2p, (d) S 2p, (e) C 1s, and (f) O 1s.

latter in the shoulder peak might originate from oxygen uptake from the environment, water vapor or carbonaceous species.[27]

To evaluate the magnetic properties of the prepared CS/CF-CNTs and CF-CNTs nanocomposites, the magnetization curve was measured at room temperature. As shown in Fig. 5, the saturation magnetization values of CS/CF-CNTs and CF-CNTs are 12.78 emu g^{-1} and 32.6 emu g^{-1}, respectively. These values indicate that the materials are superparamagnetic.[28] By comparing the magnetization curves, it can be observed that the magnetization ability of CS/CF-CNTs is lower than that of pure
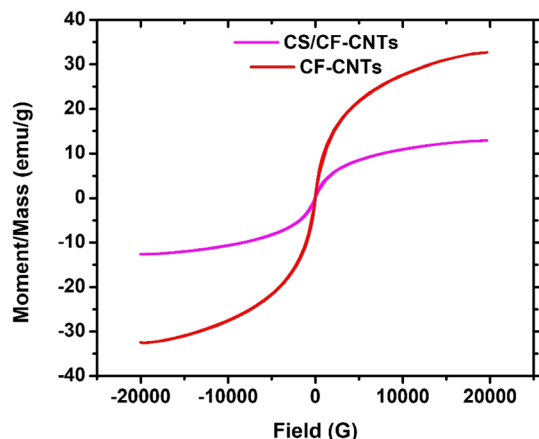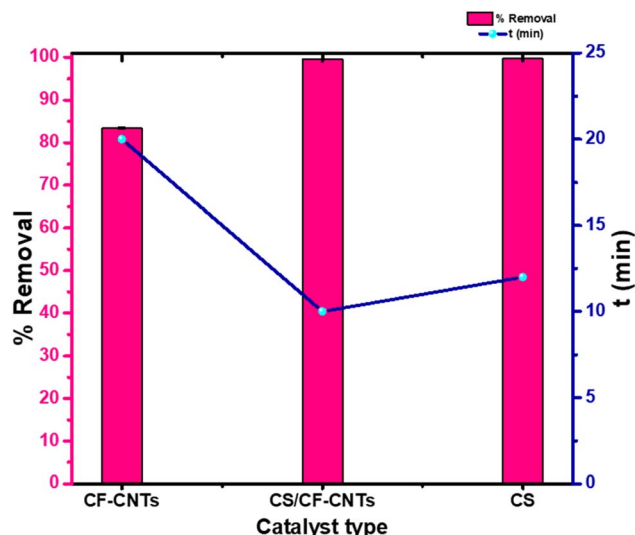
Fig. 5 VSM plots for CS/CF-CNTs and CF-CNTs.

Fig. 7 Comparison between the degradation performance of several catalysts at 10 mg/100 mL catalyst dose and 60 mg/100 mL PMS at normal pH conditions for a Rhodamine-B concentration of 50 ppm.

CF-CNTs. The decreased magnetic intensity of CS/CF-CNTs may be attributed to the CS coating. Nevertheless, the good magnetic responsiveness of the as-prepared nanocomposite enabled it to be separated conveniently with an external magnetic field, facilitating its collection and reuse.

The nitrogen adsorption–desorption isotherms of the CS/CF-CNTs hybrid nanocomposite were also obtained to determine its specific surface area (Fig. 6a) and its PSD (pore size distribution) (Fig. 6b). Following the classification scheme of the International Union of Pure and Applied Chemistry (IUPAC), the synthesized nanocomposite exhibits a type IV isotherm with a minor hysteresis loop, indicating the prevalence of mesopores along with some macropores, likely attributable to unoccupied spaces within the hybrid nanocomposite.[29] This is supported by the PSD shown in Fig. 6b. As a result, the BET surface area was determined to be 34.7 m^2 g^{-1}, with the average pore size estimated at 22.4 nm and the pore volume at 0.175 cm^3 g^{-1} using the BJH equation. The above characterization findings indicate that the CS/CF-CNTs hybrid nanocomposite possesses a mesoporous crystalline structure.

Fig. 7 shows a comparison between the different examined catalysts in their percent removal and time needed for the degradation of Rhodamine-B. As shown in the figure, CF-CNTs

gave the lowest percent removal of about 83% in 20 min, whilst both CS and CS/CF-CNTs gave almost the same percent removal (about 99.5%) after 12 and 10 min, respectively. This indicates that the inclusion of magnetic cobalt ferrite did not affect the removal efficiency of the nanocomposite, but did affect the degradation rate. In this work, we focused on the catalytic degradation of Rhodamine-B using the CS/CF-CNTs nanocomposite as it provides a faster degradation rate than the other tested catalysts, and in addition it can be easily removed from wastewater by applying a magnetic field.

3.1.1. Effect of PMS and catalyst concentration. Fig. 8a shows the effect of increasing the PMS concentration at a constant catalyst concentration of 10 mg/100 mL. When the PMS concentration was increased three-fold, the degradation time dropped by one third, *i.e.*, the degradation time decreased from 30 min for an 86.9% degradation at 20 mg/100 mL PMS to 10 min for a 99.7% degradation at 60 mg/100 mL PMS, which is an indication of the role of PMS in generating radicals and thus
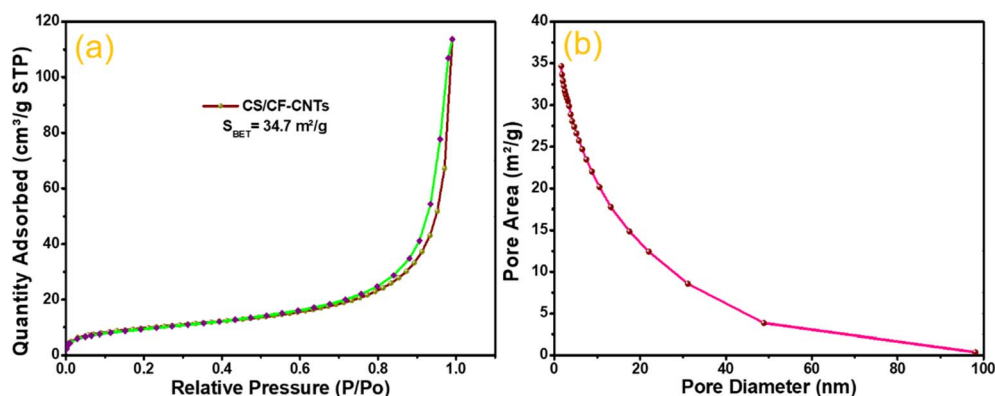

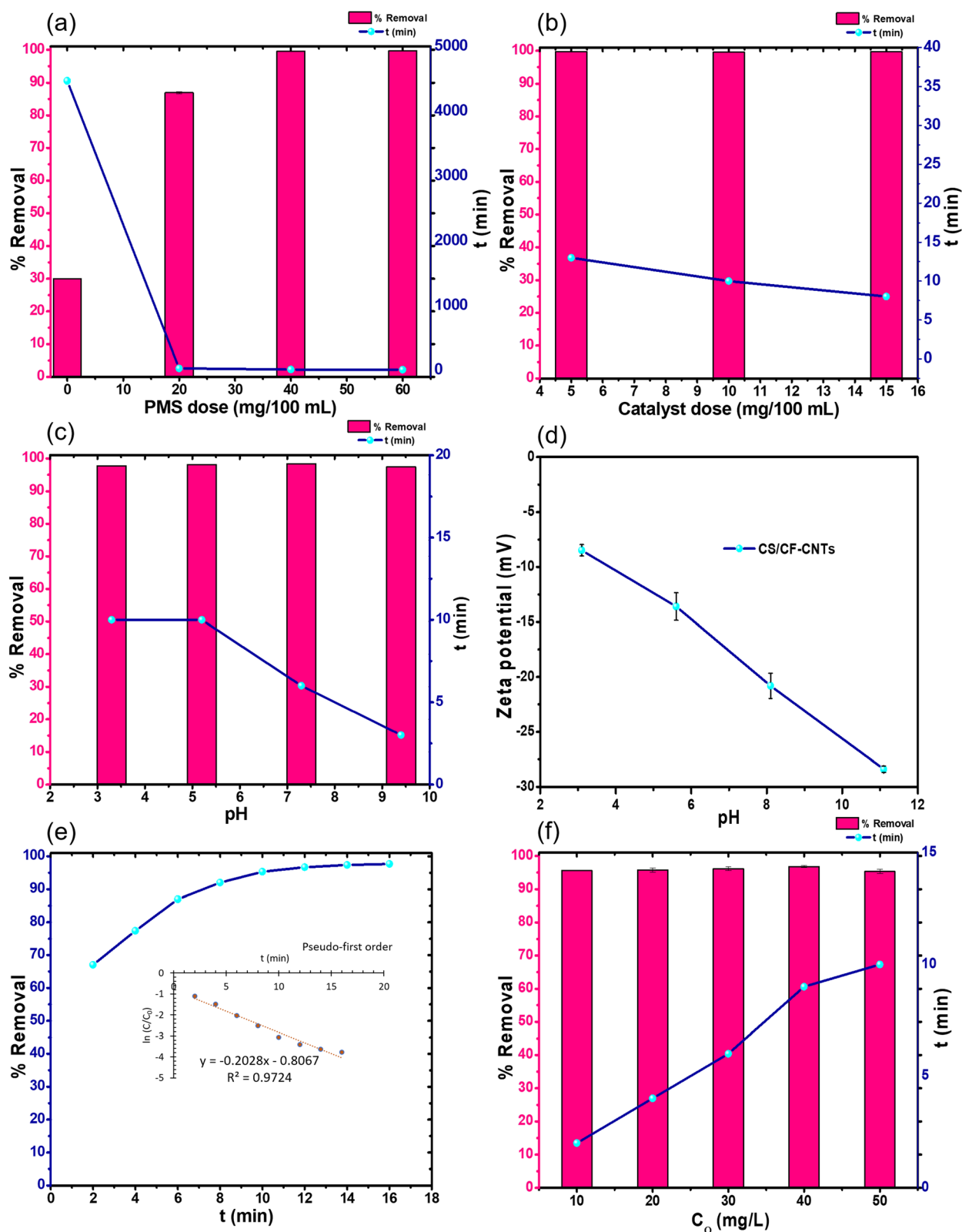Fig. 6 BET isotherm (a) and pore size distribution (b) of CS/CF-CNTs.

Fig. 8 The effect of PMS dosage at a catalyst concentration of 10 mg/100 mL, at pH 3.3 and 50 mg L^{-1} Rhodamine-B (a). The effect of catalyst concentration at a PMS dose of 60 mg/100 mL, at pH 3.3, and 50 mg L^{-1} Rhodamine-B (b). The effect of pH on Rhodamine-B degradation at a PMS and catalyst concentration of 60 and 10 mg/100 mL, respectively, with 50 mg L^{-1} Rhodamine-B (c). DLS measurement of the CS/CF-CNTs at different pH values (d). The effect of contact time of the catalyst and PMS with Rhodamine-B at a PMS and catalyst concentration of 60 and 10 mg/100 mL, respectively, and at pH 3.3 and 50 mg L^{-1} Rhodamine-B. Inset: pseudo-first-order linear kinetic plot. (e) The effect of increasing the initial concentration of Rhodamine-B on the degradation process with 60 mg/100 mL PMS and 10 mg/100 mL catalyst at pH 3.3 (f).

reducing the degradation time. This is in alignment with a previous report about Co–Mn layered double hydroxides with PMS, in which increasing the PMS concentration led to an increase in the degradation rate of Acid Orange G.[30] Thus, the PMS concentration of 60 mg/100 mL was applied in further studies. Notably, no remarkable decrease in degradation efficiency was obtained using PMS alone. To a similar extent, when the catalyst dose was increased from 5 to 15 mg/100 mL (Fig. 8b), the time required for almost complete degradation (99%) decreased from 13 min to 8 min. This could be due to the increase in the active sites available for the reaction with PMS to generate more reactive radicals and enhance the catalytic degradation. This concurs with the results reported for the use of manganese oxide octahedral molecular sieve/PMS for the degradation of acid orange 7 at higher catalyst concentrations.[31] However, due to the insignificant difference between the degradation time at 10 mg/100 mL catalyst (10 min) and that at 15 mg/100 mL catalyst (8 min), the catalyst concentration of 10 mg/100 mL was applied in further studies. It should be noted that the concentration of the catalyst should always be less than that of PMS; otherwise, the catalyst will react with the produced radicals, leading to a decrease in the removal efficiency.[32]

3.1.2. Effect of pH. As the PMS degradation process is affected by the initial pH of the solution, the effect of pH was studied in the textile wastewater pH range[33] of 3.3 to 9.4; pH 3.3 is the normal pH without adjustment. As depicted in Fig. 8c, almost complete degradation was obtained over the whole pH range. The time for complete degradation decreased from 10 min at pH 3.3 to 3 min at pH 9.4. At pH values below 6, electrostatic chemical interactions *via* electron transfer could possibly take place between the negatively charged catalyst, as confirmed from the zeta potential measurements (Fig. 8d), and the positively charged dye, while at pH values above 6, possible physical interactions are likely to occur between the negatively charged catalyst and the neutral dye (https://chemicalize.com/, accessed Feb 4th, 2024). The degradation efficiency and degradation time shown herein are higher than those previously reported for the degradation of Brilliant Blue FCF using Fe_3O_4–TiO_2/PMS, where only 61% decolorization was attained at pH 6 using 0.4 g L^{-1} catalyst and 1.5 mM PMS

after 60 min.[34] Thus, this catalyst could be efficiently applied in basic, neutral, and acidic media, which facilitates its application in real wastewaters. For practicality and ease of operation, the pH of the dye solution without adjustment (pH 3.3) was applied in the rest of the study. The kinetics of degradation followed the pseudo-first order model with an R^2 value of 0.9724 (Fig. 8e). It should be noted that the pH of the Rhodamine-B solution remained almost constant (at pH 2.8) after the degradation.

3.1.3. Effect of initial concentration. The effect of the initial concentration of Rhodamine-B dye on the degradation was investigated in the range of 10 to 50 mg L^{-1}, as depicted in Fig. 8f. Complete degradation of the dye was attained over the whole range of initial concentrations; however, the time required for complete degradation increased from 2 min at 10 mg L^{-1} to 10 min at 50 mg L^{-1}, possibly due to saturation of the active sites on the catalyst surface, which, in turn, limited the diffusion of the dye molecules to and from the catalyst surface.[35] Thus, a longer time is required for the complete degradation of the dye with increasing initial dye concentration. These findings are similar to those reported for the degradation of methylene blue by manganese cobaltite nanoparticles/PMS, where increasing methylene blue concentrations required longer times for complete degradation.[35] Notably, the reported analyte-to-PMS molar ratios range from 1 : 2 to 1 : 250; the molar ratio used herein is 1 : 51, which is in accordance with previously published literature.[36]

3.1.4. Degradation in tap water and the presence of salts. The degradation of Rhodamine-B dye was studied in tap water and compared to that in distilled water, as shown in Fig. 9a. Complete degradation was achieved in both tap water and distilled water; however, the degradation time for tap water was 0.5 min as compared to 2 min for distilled water. This finding was also observed in a previous report on the degradation of naproxen by g-C_3N_4 and was attributed to the presence of divalent magnesium and calcium cations as well as chloride ions in tap water, which could have played a role in the degradation process.[37] Additionally, the efficiency and time of the degradation of methyl red dye was enhanced in tap water relative to distilled water after applying Fe_3O_4/ZrO_2 nanoparticles
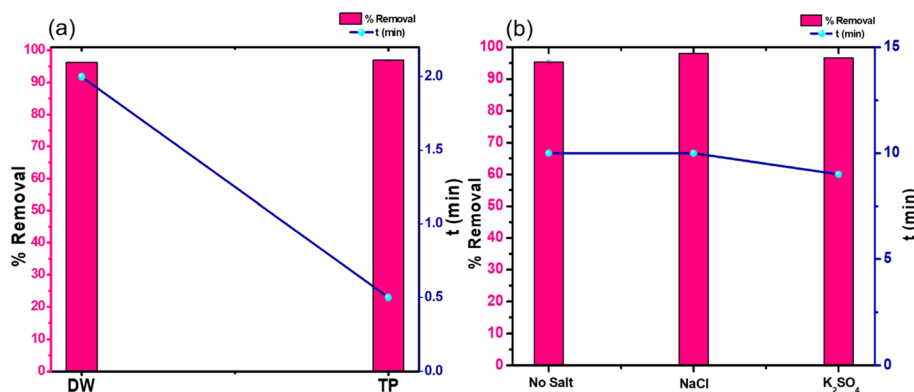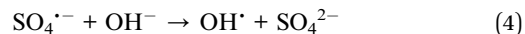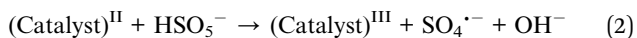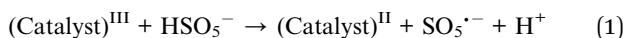

Fig. 9 Degradation of Rhodamine-B in tap water (TP) *vs.* distilled water (DW) at respective PMS and catalyst concentrations of 60 and 10 mg/ 100 mL and pH 3.3 (a), Effect of different salts on the removal and degradation time (b).

owing to the presence of mineral ions in tap water.[38] It is also possible that the presence of the mineral ions in tap water changed the ionic environment surrounding the catalyst surface and consequently enhanced the interaction between the dye and the catalyst.

The removal efficiency of Rhodamine-B by the catalyst with PMS was investigated in the presence of the salts NaCl and K_2SO_4 at a concentration of 5 mM (as shown in Fig. 9b). The results indicated that the percentage removal and degradation times remained almost constant or slightly improved, suggesting that the presence of salts did not influence the degradation performance of the catalyst. This finding suggests that there was no competition between the salts and Rhodamine-B. Previous studies have stated that Cl^- reacts with HSO_5^- to produce more active species, thereby enhancing removal efficiencies and reducing degradation times.[39] Additionally, Cl^- might generate $HOCl/Cl_2$, which could accelerate dye degradation or react with sulfate radicals to generate the less-reactive $Cl^{\bullet}$.[40] Although sulfate salts have been reported to decrease reaction rates and deactivate the catalyst surface, this effect was not observed in this study, possibly because the salt concentration used was lower than in previous reports.[41]

3.1.5. Elucidation of the reaction mechanism. Based on the experimental results, it is suggested that the CS/CF-CNTs may trigger the activation of PMS, as indicated in previous work.[42] Initially, Rhodamine-B likely adsorbs onto the surface of the nanocomposite when it is introduced into the untreated solution. This adsorption can take place chemically or physically, depending on the solution pH. Upon exposure to PMS, the surface of the CS/CF-CNTs hybrid nanocomposite is activated, facilitating the release of radical species ($SO_4^{\bullet-}$, $^{\bullet}OH$), similar to the catalytic behavior of transition metal ions[43] (eqn (1)–(4)). This activation leads to the generation of $^{\bullet}OH$ through the reaction of $SO_4^{\bullet-}$ with OH^- or H_2O (eqn (3) and (4)). The bivalent (II) metal ions within the CS/CF-CNTs catalyst play a crucial role in releasing $SO_4^{\bullet-}$ from PMS and subsequently oxidizing into their trivalent forms. Following this, PMS reduces the trivalent (III) metal ions back to their bivalent (II) states, resulting in the formation of less-active $SO_5^{\bullet-}$. However, this reduction step occurs relatively slowly, leading to a low content of bivalent metal ions (II) during the catalytic reaction. The free radicals attack the pollutant molecules, causing the pollutants to be decomposed into small molecules and finally mineralized into carbon dioxide and water. The presence of CNTs aids in dispersing the CS/CF, exposing more active sites of the bivalent (II) metal ions. Consequently, the CNTs assist in the regeneration of bivalent (II) metal ions, enhancing the catalytic potential and stability for PMS activation. This synergistic interaction between CS/CF and CNTs significantly improves the catalytic efficiency and stability for PMS activation.

$$(Catalyst)^{III} + HSO_5^- \rightarrow (Catalyst)^{II} + SO_5^{\bullet-} + H^+ \qquad (1)$$

$$(Catalyst)^{II} + HSO_5^- \rightarrow (Catalyst)^{III} + SO_4^{\bullet-} + OH^- \qquad (2)$$

$$SO_4^{\bullet-} + H_2O \rightarrow OH^{\bullet} + SO_4^{2-} + H^+ \qquad (3)$$

$$SO_4^{\bullet-} + OH^- \rightarrow OH^{\bullet} + SO_4^{2-} \qquad (4)$$

$$SO_4^{\bullet-}/OH^{\bullet} + Dye \rightarrow H_2O + CO_2 \text{ (degradation product)} \qquad (5)$$

This reaction mechanism was confirmed by quenching experiments in which 1 M ethanol and 1 M TBA were applied as quenching agents. It is well known that TBA quenches hydroxyl radicals ($k_1 = (3.8–7.6) \times 10^8$) while ethanol quenches both hydroxyl ($k_1 (OH^{\bullet}, ethanol) = 1.2–2.8 \times 10^9 \text{ M}^{-1} \text{ s}^{-1}$) and sulfate radicals ($k_1 (SO_4^{\bullet-}, ethanol) = 1.6–7.8 \times 10^7 \text{ M}^{-1} \text{ s}^{-1}$).[11] As can be seen from Fig. 10, TBA decreased the percent removal of Rhodamine-B by about 6.8%, while ethanol decreased the percent removal by 9%. This could imply that both sulfate radicals and hydroxyl radicals were involved in the reaction mechanism, with sulfate radicals being slightly more dominant. Notably, the reduction in percent removal by ethanol or TBA quenching was not substantial despite applying a 1 M concentration of each reagent. It could be that the degradation reaction rate is faster than the ethanol or TBA quenching rate, leading to minimal effects of quenching on the percent removal, or that the amount of the quenching agent was not sufficient to produce a prominent effect.[10]

3.1.6. Reusability. The reusability of the catalyst was examined for four consecutive cycles using 10 mg L^{-1} of the dye, separating the catalyst with a magnetic field, and applying it for the next cycle (Fig. 11a). The degradation efficiency of the catalyst was not affected; however, the degradation rate decreased with increasing the number of cycles, from 2 min in the first cycle to about 35 min in the fourth cycle. The reason for the decline in the degradation rate could be ascribed to the leaching of catalyst molecules as well as the masking of active sites by the degradation products of the dye.[44] Moreover, Fig. 11b depicts the FTIR spectra of the CS/CF-CNTs catalyst composite before and after four cycles of Rhodamine-B degradation. The very slight peak shift observed after degradation
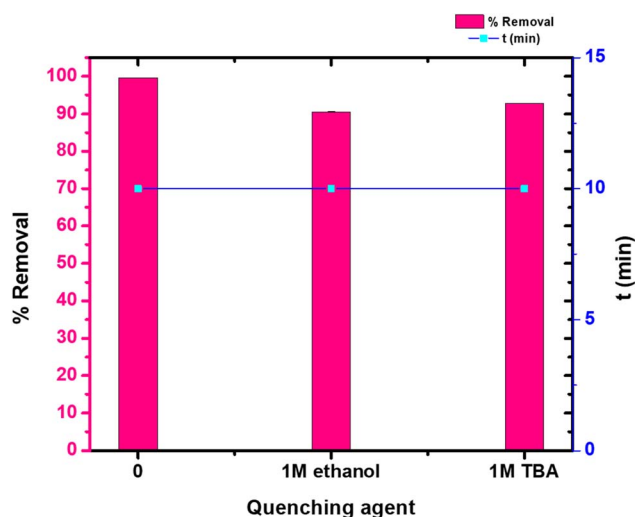

Fig. 10 Effect of radical scavengers on Rhodamine-B degradation. Reaction conditions: 10 mg/100 mL catalyst dose and 60 mg/100 mL PMS at normal pH conditions for a Rhodamine-B concentration of 50 ppm.
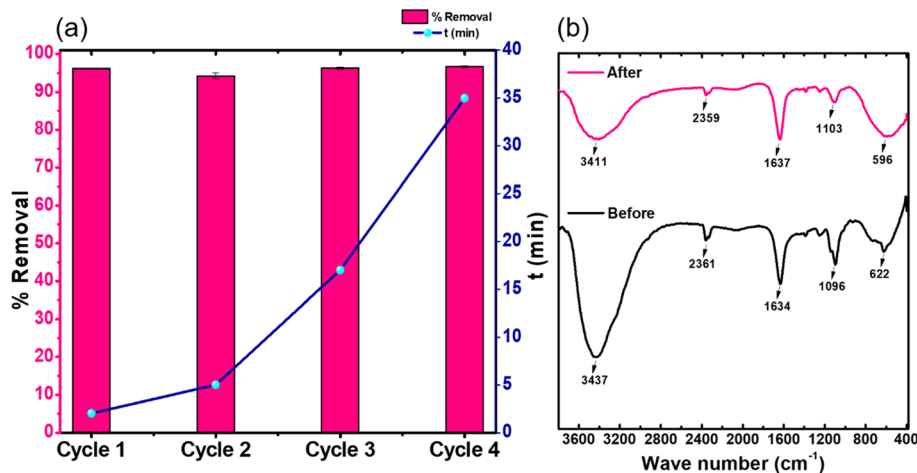
Fig. 11 Reusability of 10 mg/100 mL catalyst for the degradation of 10 mg L^{-1} Rhodamine-B at a PMS concentration of 60 mg/100 mL and pH 3.3 (a). FT-IR spectra before and after degradation (b).

Table 1 Selected cobalt-based catalysts coupled with PMS for the degradation of Rhodamine-B dye

Catalyst	Initial concentration of dye	Conc. of catalyst	Conc. of PMS	pH	%R	Ref.
CoS-rGO	14.37 mg L^{-1}	0.25 g L^{-1}	0.0056 g L^{-1}	3–10	100% in 8 min	47
Co-doped hydroxyapatite	40 mg L^{-1}	0.2 g L^{-1}	0.045 g L^{-1}	5.5	93.3% in 12 min	48
Co/nitrogen-doped CNTs annealed at 700 °C	20 mg L^{-1}	0.02 g L^{-1}	0.06 g L^{-1}	5.67	99.05% in 7 min	49
CoFe/SBA-15 calcined at 700 °C	5 mg L^{-1}	0.1 g L^{-1}	—	No adjustment	>98% in 60 min	50
FeCo-LDH	20 mg L^{-1}	0.2 g L^{-1}	0.15 g L^{-1}	No adjustment	>98% in 10 min	51
CS/CF-CNTs	50 mg L^{-1}	0.1 g L^{-1}	0.6 g L^{-1}	No adjustment	>98% in 10 min	This work

indicates alterations in the chemical environment of the functional groups, possibly due to the formation of new bonds between the catalyst and the degradation products. Although, there is a decrease in peak intensity after degradation, the vibration peaks of CS/CF-CNTs after regeneration of the catalyst remained mostly unchanged compared to the peaks shown for the fresh catalyst. This indicates that the CS/CF-CNTs catalyst possesses excellent catalytic stability and reusability.

3.1.7. Stability of the catalyst. The content of the cobalt and iron ions leached into the water was studied after conducting a catalytic degradation experiment using 10 mg catalyst and 60 mg PMS in 100 mL of 50 ppm Rhodamine-B solution; the concentration of cobalt and iron in the treated water was then measured using ICP. It was found that the concentration of leached iron was about 0.257 mg L^{-1}, while that of cobalt was about 0.13 mg L^{-1}. For iron, the maximum acceptable limit determined by the Minnesota Department of Health is 0.3 mg L^{-1},[45] which shows that the amount of iron leached from the composite is below the maximum acceptable limit and thus ensures the safety of using the composite with regard to iron leaching. Similarly, the content of leached cobalt is within the permissible limits of cobalt in freshwater, which should not exceed 0.11 mg L^{-1} as per previously reported guidelines.[46]

4. Comparison with literature

Table 1 lists some examples of cobalt-based catalysts that were coupled with PMS for the degradation of Rhodamine-B. The results show that the activity of our catalyst exceeded that of Co-doped hydroxyapatite, FeCo-LDH, CoFe/SBA-15 and CoS-rGO in terms of catalyst/dye weight ratio. All listed catalysts showed degradation within an 8 to 15 min time frame except for CoFe/SBA-15, which required 60 min.

5. Conclusions

In this study, a magnetic CS/CF-CNTs catalyst was successfully synthesized *via* a simple hydrothermal process and exhibited excellent performance in activating PMS to degrade Rhodamine-B, a representative organic dye. The catalyst was fully characterized by various techniques to evaluate its physicochemical properties. Compared to CF-CNTs and CNTs, the CS/CF-CNTs nanocomposite displayed notably enhanced catalytic activity in removing Rhodamine-B with a degradation efficiency of >95% in only 10 min. The influence of different parameters on the degradation of Rhodamine-B was investigated, revealing pH, PMS concentration, and initial Rhodamine-B concentration as critical factors affecting the

degradation rate. For example, by increasing the concentration of PMS from 20 to 60 mg/100 mL, the degradation time was decreased from 30 min to 10 min while the degradation efficiency was enhanced from 86.9% to 99.7%. Moreover, owing to its exceptional recyclability, this catalyst could be easily separated using an external magnet and reused multiple times, indicating its practical application value. This work provides a new strategy for developing an efficient reusable nanocatalyst for pollutant degradation *via* an environmentally safe process in which the magnetic catalyst is easily collected from water, thus mitigating its environmental impact.

Data availability

The data supporting the findings of this study, including experimental results and application outputs, are available in the manuscript. Additional data are available upon reasonable request.

Conflicts of interest

The authors declare no conflicts of interest.

Acknowledgements

References

1 Z. Chen, G. Wu, Y. Wu, Q. Wu, Q. Shi, H. H. Ngo, O. A. V. Saucedo and H.-Y. Hu, Water Eco-Nexus Cycle System (WaterEcoNet) as a key solution for water shortage and water environment problems in urban areas, *Water Cycle*, 2020, **1**, 71–77.

2 S. Khan, M. Naushad, M. Govarthanan, J. Iqbal and S. M. Alfadul, Emerging contaminants of high concern for the environment: Current trends and future research, *Environ. Res.*, 2022, **207**, 112609.

3 A. A. Al-Gheethi, Q. M. Azhar, P. S. Kumar, A. A. Yusuf, A. K. Al-Buriahi, R. M. S. R. Mohamed and M. M. Al-Shaibani, Sustainable approaches for removing Rhodamine B dye using agricultural waste adsorbents: A review, *Chemosphere*, 2022, **287**, 132080.

4 K. Mahdavi, S. Zinatloo-Ajabshir, Q. A. Yousif and M. Salavati-Niasari, Enhanced photocatalytic degradation of toxic contaminants using Dy2O3-SiO2 ceramic nanostructured materials fabricated by a new, simple and rapid sonochemical approach, *Ultrason. Sonochem.*, 2022, **82**, 105892.

5 J. Shah, M. Rasul Jan, A. Haq and Y. Khan, Removal of Rhodamine B from aqueous solutions and wastewater by walnut shells: kinetics, equilibrium and thermodynamics studies, *Front. Chem. Sci. Eng.*, 2013, **7**, 428–436.

6 W. Xiao, Z. N. Garba, S. Sun, I. Lawan, L. Wang, M. Lin and Z. Yuan, Preparation and evaluation of an effective activated carbon from white sugar for the adsorption of rhodamine B dye, *J. Cleaner Prod.*, 2020, **253**, 119989.

7 R. A. Nasr and E. A. Ali, Polyethersulfone/gelatin nano-membranes for the Rhodamine B dye removal and textile industry effluents treatment under cost effective condition, *J. Environ. Chem. Eng.*, 2022, **10**, 107250.

8 P. Zawadzki and M. Deska, Degradation Efficiency and Kinetics Analysis of an Advanced Oxidation Process Utilizing Ozone, Hydrogen Peroxide and Persulfate to Degrade the Dye Rhodamine B, *Catalysts*, 2021, **11**, 974.

9 Y. Deng and R. Zhao, Advanced oxidation processes (AOPs) in wastewater treatment, *Curr. Pollut. Rep.*, 2015, **1**, 167–176.

10 F. Ghanbari and M. Moradi, Application of peroxymonosulfate and its activation methods for degradation of environmental organic pollutants, *Chem. Eng. J.*, 2017, **310**, 41–62.

11 M. Abdel-Salam and T. Yoon, Cobalt-ferrite/Ag-fMWCNT hybrid nanocomposite catalyst for efficient degradation of synthetic organic dyes via peroxymonosulfate activation, *Environ. Res.*, 2022, **205**, 112424.

12 D. Xu, X. Sun, X. Zhao, L. Huang, Y. Qian, X. Tao and Q. Guo, Heterogeneous Fenton degradation of rhodamine B in aqueous solution using Fe-loaded mesoporous MCM-41 as catalyst, *Water, Air, Soil Pollut.*, 2018, **229**, 1–9.

13 Q. Gao, G. Wang, Y. Chen, B. Han, K. Xia and C. Zhou, Utilizing cobalt-doped materials as heterogeneous catalysts to activate peroxymonosulfate for organic pollutant degradation: a critical review, *Environ. Sci. Water Res. Technol.*, 2021, **7**, 1197–1211.

14 S. Mishra and B. Sundaram, Efficacy and challenges of carbon nanotube in wastewater and water treatment, *Environ. Nanotechnol. Monit. Manage.*, 2023, **19**, 100764.

15 T. Li, A. O. Omoniyi, Y. Wang, X. Hu and Z. Su, Enhancing dye degradation using a novel cobalt metal–organic framework as a peroxymonosulfate activator, *Dalton Trans.*, 2024, **53**, 3523–3533.

16 A. B. Hamou, M. Enneiymy, S. Farsad, A. Amjlef, A. Chaoui, N. Nouj, A. Majdoub, A. Jada, M. Ez-zahery and N. El Alem, Novel chemically reduced cobalt-doped gC₃N₄ (CoCN-x) as a highly heterogeneous catalyst for the super-degradation of organic dyes via peroxymonosulfate activation, *Mater. Adv.*, 2024, **5**, 1960–1976.

17 Y. M. Moustafa, A. M. Al-Sabagh, S. A. Younis, M. M. Khalil and M. O. Abdel-Salam, Preparation of magnetic carbon nanotube nanocomposite for enhancing the separation of dissolved hydrocarbon from petroleum wastewater, *J. Environ. Chem. Eng.*, 2017, **5**, 2240–2250.

18 B. Babić-Stojić, V. Jokanović, D. Milivojević, Z. Jagličić, D. Makovec, N. Jović and M. Marinović-Cincović, Magnetic and structural studies of CoFe2O4 nanoparticles suspended in an organic liquid, *J. Nanomater.*, 2013, **2013**, 11.

19 L.-L. Ren, L.-H. Wang, Y.-F. Qin and Q. Li, One-Pot Synthesized Amorphous Cobalt Sulfide With Enhanced

Electrochemical Performance as Anodes for Lithium-Ion Batteries, *Front. Chem.*, 2022, **9**, 818255.

20 H. Wang, J. Ma, S. Liu, L. Nie, Y. Chai, X. Yang and R. Yuan, CoS/CNTs hybrid structure for improved performance lithium ion battery, *J. Alloys Compd.*, 2016, **676**, 551–556.

21 Q. Wang, L. Jiao, H. Du, W. Peng, Y. Han, D. Song, Y. Si, Y. Wang and H. Yuan, Novel flower-like CoS hierarchitectures: one-pot synthesis and electrochemical properties, *J. Mater. Chem.*, 2011, **21**, 327–329.

22 X. Wang, Y. Xiao, D. Su, L. Zhou, S. Wu, L. Han, S. Fang and S. Cao, High-quality porous cobalt monoxide nanowires@ ultrathin manganese dioxide sheets core-shell nanowire arrays on Ni foam for high-performance supercapacitor, *Electrochim. Acta*, 2016, **194**, 377–384.

23 Y. Wang, T. Zhu, Y. Zhang, X. Kong, S. Liang, G. Cao and A. Pan, Rational design of multi-shelled CoO/Co 9 S 8 hollow microspheres for high-performance hybrid supercapacitors, *J. Mater. Chem. A*, 2017, **5**, 18448–18456.

24 S. J. Patil, J. H. Kim and D. W. Lee, Graphene-nanosheet wrapped cobalt sulphide as a binder free hybrid electrode for asymmetric solid-state supercapacitor, *J. Power Sources*, 2017, **342**, 652–665.

25 J. Wang, Y. Zhang, J. Wang, L. Gao, Z. Jiang, H. Ren and J. Huang, Preparation of cobalt sulfide@ reduced graphene oxide nanocomposites with outstanding electrochemical behavior for lithium-ion batteries, *RSC Adv.*, 2020, **10**, 13543–13551.

26 J. Huang, W. Wang, X. Lin, C. Gu and J. Liu, Three-dimensional sandwich-structured NiMn2O4@ reduced graphene oxide nanocomposites for highly reversible Li-ion battery anodes, *J. Power Sources*, 2018, **378**, 677–684.

27 W. P. Wang, H. Yang, T. Xian and L. J. Jiang, XPS and magnetic properties of CoFe2O4 nanoparticles synthesized by a polyacrylamide gel route, *Mater. Trans.*, 2012, **53**, 1586–1589.

28 T. George, A. Sunny and T. Varghese, *IOP Conf. Ser.:Mater. Sci. Eng.*, 2015, **73**, 012050.

29 M. M. Rahman, A. Z. Shafiullah, A. Pal, M. A. Islam, I. Jahan and B. B. Saha, Study on Optimum IUPAC Adsorption Isotherm Models Employing Sensitivity of Parameters for Rigorous Adsorption System Performance Evaluation, *Energies*, 2021, **14**, 7478.

30 X. Zhao, C. Niu, L. Zhang, H. Guo, X. Wen, C. Liang and G. Zeng, Co-Mn layered double hydroxide as an effective heterogeneous catalyst for degradation of organic dyes by activation of peroxymonosulfate, *Chemosphere*, 2018, **204**, 11–21.

31 S. Luo, L. Duan, B. Sun, M. Wei, X. Li and A. Xu, Manganese oxide octahedral molecular sieve (OMS-2) as an effective catalyst for degradation of organic dyes in aqueous solutions in the presence of peroxymonosulfate, *Appl. Catal., B*, 2015, **164**, 92–99.

32 M. Moazeni, S. M. Hashemian, M. Sillanpää, A. Ebrahimi and K.-H. Kim, A heterogeneous peroxymonosulfate catalyst built by Fe-based metal-organic framework for the dye degradation, *J. Environ. Manage.*, 2022, **303**, 113897.

33 D. A. Yaseen and M. Scholz, Impact of pH on the treatment of artificial textile wastewater containing azo dyes using pond systems, *Int. J. Environ. Res.*, 2019, **13**, 367–385.

34 M. A. Zazouli, F. Ghanbari, M. Yousefi and S. Madihi-Bidgoli, Photocatalytic degradation of food dye by Fe3O4–TiO2 nanoparticles in presence of peroxymonosulfate: The effect of UV sources, *J. Environ. Chem. Eng.*, 2017, **5**, 2459–2468.

35 N. T. Dung, T. V. Thu, T. Van Nguyen, B. M. Thuy, M. Hatsukano, K. Higashimine, S. Maenosono and Z. Zhong, Catalytic activation of peroxymonosulfate with manganese cobaltite nanoparticles for the degradation of organic dyes, *RSC Adv.*, 2020, **10**, 3775–3788.

36 L. W. Matzek and K. E. Carter, Activated persulfate for organic chemical degradation: a review, *Chemosphere*, 2016, **151**, 178–188.

37 M. Jimenez-Salcedo, M. Monge and M. T. Tena, The photocatalytic degradation of naproxen with g-C3N4 and visible light: Identification of primary by-products and mechanism in tap water and ultrapure water, *J. Environ. Chem. Eng.*, 2022, **10**, 106964.

38 I. Khan, N. Zada, I. Khan, M. Sadiq and K. Saeed, Enhancement of photocatalytic potential and recoverability of Fe 3 O 4 nanoparticles by decorating over monoclinic zirconia, *J. Environ. Health Sci. Eng.*, 2020, **18**, 1473–1489.

39 L. Zeng, L. Xiao, X. Shi, M. Wei, J. Cao and Y. Long, Core-shell Prussian blue analogues@ poly (m-phenylenediamine) as efficient peroxymonosulfate activators for degradation of Rhodamine B with reduced metal leaching, *J. Colloid Interface Sci.*, 2019, **534**, 586–594.

40 J. Di, R. Jamakanga, Q. Chen, J. Li, X. Gai, Y. Li, R. Yang and Q. Ma, Degradation of Rhodamine B by activation of peroxymonosulfate using Co3O4-rice husk ash composites, *Sci. Total Environ.*, 2021, **784**, 147258.

41 R. Jiang, D. Zhong, Y. Xu, H. Chang, P. Liao, Y. He and J. Zhang, Efficient degradation of rhodamine B by MoS2 modified Co-MOF derived nitrogen-doped carbon activated peroxymonosulfate, *Colloids Surf., A*, 2024, **685**, 133184.

42 C. Li, J. Wu, W. Peng, Z. Fang and J. Liu, Peroxymonosulfate activation for efficient sulfamethoxazole degradation by Fe3O4/β-FeOOH nanocomposites: Coexistence of radical and non-radical reactions, *Chem. Eng. J.*, 2019, **356**, 904–914.

43 C. Tan, N. Gao, Y. Deng, J. Deng, S. Zhou, J. Li and X. Xin, Radical induced degradation of acetaminophen with Fe3O4 magnetic nanoparticles as heterogeneous activator of peroxymonosulfate, *J. Hazard. Mater.*, 2014, **276**, 452–460.

44 P. K. Klu, M. A. N. Khan, C. Wang, J. Qi, X. Sun and J. Li, Mechanism of peroxymonosulfate activation and the utilization efficiency using hollow (Co, Mn) 3O4 nanoreactor as an efficient catalyst for degradation of organic pollutants, *Environ. Res.*, 2022, **207**, 112148.

45 Iron in Well Water, 2025, **https://www.health.state.mn.us/ communities/environment/water/wells/waterquality/iron. html#:~:text=PointofreferenceAWaterwith,10mgFLinwater.**

46 N. K. Nagpal, *Technical Report – Water Quality Guidelines For Cobalt*, 2025, **https://www2.gov.bc.ca/assets/gov/ environment/air-land-water/water/waterquality/water-quality-guidelines/approved-wqgs/cobalt_tech.pdf.**

47 L. Amirache, F. Barka-Bouaifel, P. Borthakur, M. R. Das, H. Ahouari, H. Vezin, A. Barras, B. Ouddane, S. Szunerits and R. Boukherroub, Cobalt sulfide-reduced graphene oxide: An efficient catalyst for the degradation of rhodamine B and pentachlorophenol using peroxymonosulfate, *J. Environ. Chem. Eng.*, 2021, **9**, 106018.

48 Y. Pang, L. Kong, D. Chen, G. Yuvaraja and S. Mehmood, Facilely synthesized cobalt doped hydroxyapatite as hydroxyl promoted peroxymonosulfate activator for degradation of Rhodamine B, *J. Hazard. Mater.*, 2020, **384**, 121447.

49 J. Cheng, N. Wei, Y. Wang, Y. Long and G. Fan, Direct transformation of bulk cobalt foam into cobalt nanoparticles encapsulated in nitrogen-doped carbon nanotubes for peroxymonosulfate activation toward rhodamine B degradation, *Sep. Purif. Technol.*, 2021, **277**, 119441.

50 L. Hu, F. Yang, L. Zou, H. Yuan and X. Hu, CoFe/SBA-15 catalyst coupled with peroxymonosulfate for heterogeneous catalytic degradation of rhodamine B in water, *Chin. J. Catal.*, 2015, **36**, 1785–1797.

51 C. Gong, F. Chen, Q. Yang, K. Luo, F. Yao, S. Wang, X. Wang, J. Wu, X. Li and D. Wang, Heterogeneous activation of peroxymonosulfate by Fe–Co layered doubled hydroxide for efficient catalytic degradation of Rhoadmine B, *Chem. Eng. J.*, 2017, **321**, 222–232.